Available online at www.sciencedirect.com

ScienceDirect

Procedia Engineering 00 (2015) 000–000

Procedia Engineering

www.elsevier.com/locate/procedia

6th Fatigue Design conference, Fatigue Design 2015

Commentaire [S1]: Elsevier to update with volume and page numbers.

Fatigue life from kurtosis controlled excitations

Frédéric Kihm[a]*, Neil S. Ferguson[b], Jérôme Antoni[c]

[a]*HBM-nCode Products Division, Technology Center, Brunel Way, Catcliffe, Rotherham, S60 5WG, UK*
[b]*Institute of Sound and Vibration Research, University of Southampton, Southampton SO17 1BJ, UK*
[c]*Laboratoire Vibrations Acoustique, University of Lyon, 69000 Lyon, France*

Abstract

Components of ground and flight vehicles are subjected to random vibration excitations. A common approach to qualify such components is to expose them to a random Gaussian excitation, defined by the power spectral density (PSD) of the vibration under consideration.
In real life, however, it is common to experience non-Gaussian acceleration inputs such as road irregularities in the automotive world or turbulent pressure fluctuations for the aerospace sector. Traditional Gaussian random test signals do not accurately represent the bursts and peaks seen in service use. The consequence of not using the right type of test signal during vibration testing of the product leads to higher field failure rates and added warranty costs.
Modern controllers can generate non-Gaussian excitation signals with a given PSD and kurtosis. A simulation with kurtosis control makes the vibration test more realistic and therefore closer to real-world excitations.
This paper addresses the question of linking fatigue damage with the prescribed input kurtosis. Direct applications of these results include improved fatigue life estimations and a method to accelerate shaker tests by generating high kurtosis, non-Gaussian drive signals.
The algorithm is validated using numerical simulations and a case study illustrates the application of the method.

Peer-review under responsibility of CETIM.

Keywords: fatigue; vibration; random; kurtosis; non-Gaussian; nonstationary; linear filter

* Corresponding author. Tel.: +33 130182020; fax: +33 130182019.
E-mail address: Frederic.kihm@hbmncode.com

1877-7058
Peer-review under responsibility of CETIM.

1. Introduction

In all industrial sectors e.g. Automotive, Aerospace, Energy, etc. components are designed to withstand the real operational conditions to which they will be subjected during their service life. A fatigue resistant design may reduce warranty costs and unnecessary maintenance, increase safety and reliability and will yield a better corporate reputation.

1.1. Typical qualification tests on shakers: random PSD

Shaker tests are performed to qualify the endurance of a product. In order to replicate the same failure mechanism as in real conditions, the test specification must be representative of the service loads. When running a random vibration tests, the input excitation is typically defined as a Power Spectrum Density (PSD). Example PSD's from MIL STD 810 [3] are given in Fig. 1.

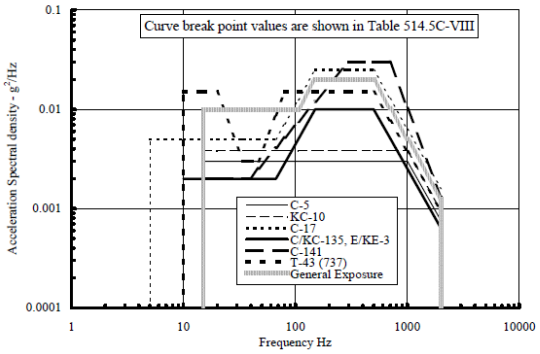

Fig. 1: Example PSD profiles from the military standard MIL STD 810 [3]

From the PSD profile, an excitation signal is generated by the controller to drive the shaker. The reproduced signal is meant to be random stationary and Gaussian.

1.2. Virtual vibration endurance tests

Durability simulations based on Finite Element Analysis (FEA) can help optimizing the design of a component. It allows hypothetical scenarios to be considered in order to select the optimum material, to choose the minimum thickness, etc. required to fulfill a target in terms of service life.

Durability simulations can limit drastically the number of prototypes in the Design phase. At the qualification stage, if the test article fails during the qualification test, FEA-based durability simulations can help understand why. Also, it can assist in assessing what the margins are if the qualification test is successful.

When a linear system is excited by a random stationary and Gaussian signal, the spectral and statistical characteristics of the response are known. If the linear system is a mechanical device and the excitation is the acceleration signal produced by a shaker, then the stress response can be derived in terms of both its Power Spectral Density and its Probability Density Function. Statistical methods exist to derive the distribution of peaks and valleys in the response and to approximate the distribution of the Rainflow ranges [18].

The benefits of such a statistical approach are:

- performance - since there is no need to perform long time domain realisations
- accuracy - since the distributions obtained are smooth with well-defined tails

Fig. 2 illustrates both benefits by comparing the resulting Rainflow histogram obtained from long time domain simulations versus the results from a statistical approach.

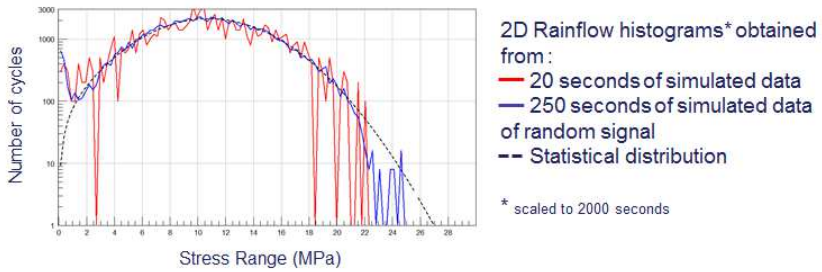

Fig. 2: Rainflow cycle histograms for various time domain realizations versus the spectral approach

The current state of the art in virtual vibration endurance testing does not allow one to simulate kurtosis-control tests. Currently, the only way of estimating the fatigue life under non-Gaussian excitations is to perform a transient analysis. Such analysis can be accelerated by using modal superposition, but is still very demanding in terms of CPU time. It also raises the question of how long the excitation signal should be to ensure convergence on the fatigue life estimate. The time domain approach is therefore impractical and this is the main reason why a spectral approach is relevant and preferred.

This paper extends a previous study [6] by the same authors. The case of non-Gaussian loading with bursts of high amplitude excursions is further explored and a formulation giving the statistics of the response is proposed based on the theory of cyclostationary processes [1,20,17]. This paper concentrates more on statistical distributions of stress Rainflow ranges and on fatigue damage. Methodologies for deriving the statistical distributions of stress Rainflow ranges are explained for both stationary and nonstationary non-Gaussian excitations. Finally, an example illustrates the approach and compares the fatigue damage due to both types of leptokurtic excitations: stationary and nonstationary.

2. Leptokurtic excitations

The various standards for environmental tests acknowledge that most measured random vibrations do not usually conform to a Gaussian distribution of amplitudes [2,3,4]. They also warn that the measured data represent a greater damage potential than Gaussian data because of their higher probability of high amplitudes.

Kurtosis is one of the principal metrics describing non-Gaussian features of a unimodal probability distribution. It is often described as a measure of the "peakedness" of a process. The kurtosis is calculated from the fourth central moment (m_4) of a random variable x, normalized by the square of the variance (m_2), i.e,

$$\kappa = \frac{m_4}{m_2^{\,2}}, \quad m_j = \frac{1}{n}\sum_{i=1}^{n}\left[\, x_i - \mu \right]^{j} \tag{1}$$

Kurtosis of a Gaussian distribution is 3.0. A process is said to be leptokurtic if its kurtosis is higher than 3.0, and platykurtic if smaller than 3.0.

Modern shaker controllers can generate signals with high kurtosis, making the test more representative of the expected vibration environment that the test article will experience during its service life. The generated signal has the same PSD, but the signal obtained is more impulsive compared to a stationary Gaussian signal. The signal with high kurtosis exhibits higher levels than the Gaussian one. In terms of fatigue damage, it is expected that more impulses means higher expected damage for the device under test so that the test duration can be reduced while reproducing the same overall damage.

This section of the paper is concerned with the excitation signals, generally measured in acceleration. This is typically the input to the test article. There are several ways to generate random signals from a PSD and with a prescribed kurtosis value [15,16]. They can be broadly divided into two families: stationary non-Gaussian and

nonstationary non-Gaussian. Examples of stationary and nonstationary leptokurtic processes are described in the next two sections.

2.1. Stationary leptokurtic excitations

A process is said to be stationary if its statistics are not affected by a shift in the time origin. (i.e. the statistics of a time history $x(t)$ are the same as a time history $x(t + \tau)$ for all values of τ) [8]. A previous paper on the subject of non-Gaussian loads [6] explains how to generate a non-Gaussian stationary signal, showing a steady rate of instantaneous peaks. It uses a zero-memory nonlinear monotonic function $y = g(x)$ to convert a zero mean Gaussian signal $x(t)$ with a specified PSD into a non-Gaussian waveform $y(t)$ [14,15,16]. This approach is also referred to as the PDF transform technique [6,7].

2.2. Nonstationary leptokurtic excitations

Another class of high kurtosis random signals is made of non-stationary processes. Although vibration is generally of random form, it is often nonstationary. In the automotive world, this arises from changes in road surface quality or for example in the aerospace sector, gusts from atmospheric turbulence. A non-stationary process can be represented as a signal with time-varying variance, typically obtained through a modulation process.

The process for generating a non-Gaussian signal with bursts starts with the generation of a stationary Gaussian signal $x(t)$ with zero mean and variance σ^2. This signal is then amplitude modulated by a low frequency waveform $a(t)$, independent of the Gaussian signal. The non-Gaussian signal $y(t)$ can therefore be written $y(t) = a(t).x(t)$.

For the sake of simplicity, the modulating signal $a(t)$ is considered periodic. The amplitude modulation function can be made of any wave form (the "burst"), followed by a flat line such that there is a smooth continuous junction between the burst and the flat portion. If the period is T seconds and the length of the burst is T_0 seconds, the proportion of burst in a period, noted r_b, is calculated as $r_b = T_0/T$, with $T_0 \leq T$. Examples of stationary Gaussian signal $x(t)$, modulation function $a(t)$ and obtained signal $y(t)$ are illustrated in Fig. 3. Note that in this example, the burst in the modulation function is a sine wave of amplitude A and an offset B.

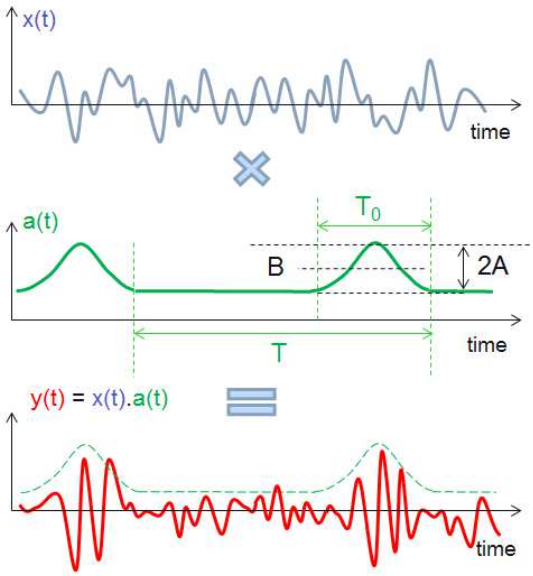

Fig. 3: Example amplitude modulation signal

Note that in real life, the bursts are not identically repeated at a constant rate. Some simplifying assumptions can be made:

- The length of the bursts pulse will be considered constant, but the bursts may appear at random instants and, as long as they don't overlap, the overall statistics of the nonstationary process remain the same.
- The amplitudes of the bursts will remain constant in this paper. Note that the pure random nature of the underlying stationary signal tends to mask the deterministic aspects of the amplitude modulation function.

Considering a given waveform for the burst in the modulating function $a(t)$, its mean value and amplitude can be calculated from the target kurtosis. The rate of bursts r_b is a user input. The value for r_b is chosen based on the type of phenomenon – more or less impulsive –to be simulated.

Note that the autocorrelation function of the amplitude modulated signal $y(t)$ is periodic [5], with period T. A process $y(t)$ is said to be cyclostationary in the wide sense if its autocorrelation is periodic [13]. The so-called cyclic spectrum of $y(t)$ can be written (see equ. 150 in [1]):

$$S_y^{p/T}(f) = \sum_k a_k a_{k-p}^* S_x\left(f - \frac{k}{T} + \frac{p}{2T}\right) \tag{2}$$

where a_k are the Fourier coefficients of the periodic modulation function $a(t)$, S_x is the PSD of $x(t)$ and the cyclic frequency $\alpha = p/T$.

Based on the cyclic spectrum $S_y^{p/T}(f)$, one can extract the statistics of the process $y(t)$ [17]. The full demonstration of this is beyond the scope of this paper.

$$\kappa_y = 3\frac{\sum_p \left| \int S_y^{p/T}(f)\,df \right|^2}{\left| \int S_y^0(f)\,df \right|^2} \tag{3}$$

In the case of simple modulation functions like a sine wave, this expression simplifies greatly and gives the kurtosis value in a closed-form formulation.

3. From excitation to stress response

In this section, the test article is considered as a linear time-invariant (LTI) system, excited by the non-Gaussian signal and producing a stress response. The response function of the LTI system is denoted $H(f)$ and its impulse response function (IRF) h_i. Fig. 4 illustrates an example system with its input and output.

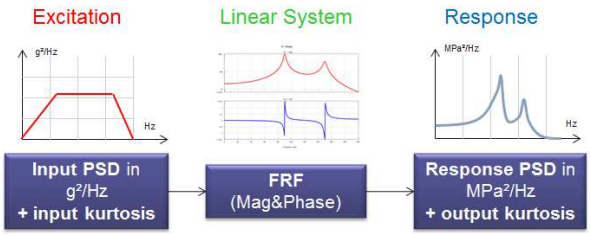

Fig. 4: Example linear system with broadband input, linear transfer function and response

The characteristics of the response of a linear system subjected to stationary random Gaussian excitations is known and largely covered in the literature [5,8,10]. There is less in the published literature on responses of linear systems to non-Gaussian random excitations.

In a previous work by Rizzi et al. [9], it was found that a leptokurtic loading having a steady rate of instantaneous, high-excursion peaks produced essentially the same response as if the load was Gaussian. In contrast, the response to a non-Gaussian loading having the same kurtosis, but with bursts of high values was found to be non-Gaussian and leptokurtic too. Over a practical range of damping, it was found that the linear response to a non-Gaussian loading was Gaussian when the period of the system impulse response is much greater than the rate of the peaks in the loading. A lower damping would typically reduce the excess kurtosis in the response.

The following sections examine the statistics of the response of a LTI system excited by firstly a stationary leptokurtic signal and then alternatively a nonstationary random leptokurtic excitation.

3.1. Stress responses due to stationary leptokurtic excitation

The stationary excitation signal is considered here to be the input to an LTI system, which basically acts as a linear convolution filter. In the case of stationary processes, the statistics of the response can be calculated from the statistics of the excitation. The formulation linking the output kurtosis κ_z with the input kurtosis κ_y and the characteristics of the input signal and the filter [6] is given in Equation (4):

$$\kappa_z = \frac{\sum f_i^4}{\left(\sum f_i^2\right)^2}\frac{\left(\sum c_i^2\right)^2}{\sum c_i^4}\left(\kappa_y - 3.0\right) + 3.0 \tag{4}$$

where c_i are the values of the autocorrelation function of the input noise and f_i are the values of the convolution of the autocorrelation function of the input noise with the IRF of the linear system.

Now consider how the behaviour of the output kurtosis is changed as a function of the characteristics of the impulse response function (IRF). The IRF corresponding to systems with very low damping will oscillate longer

than the IRF corresponding to a highly damped system. In relation to equation (5), an IRF with long decaying oscillations will minimize the term $\sum f_i^4 / \left(\sum f_i^2\right)^2$. This will lead to a lower output kurtosis for a lightly damped system than for a more heavily damped one. This behavior is consistent with the observation that the output kurtosis tends to Gaussian as the bandwidth of the filter, i.e, the amount of damping, decreases [9,12].

3.2. Stress responses due to nonstationary leptokurtic excitation

Gardner [1] gave the input-output cyclic spectra relationship for LTI systems:

$$S_z^{p/T}(f) = H\left(f + \frac{p}{2T}\right) \cdot S_y^{p/T}(f) \cdot H^*\left(f - \frac{p}{2T}\right) \tag{5}$$

where $H(f)$ is the frequency response function of the linear system and $S_z^{p/T}(f)$ and $S_y^{p/T}(f)$ the cyclic spectra for $z(t)$ and $y(t)$ respectively. $\alpha = p/T$ is the cyclic frequency, ranging over all integer multiples of the fundamental frequency $f = 1/T$ of the modulation function.

Inserting equations (2) and (5) into equation (3), one obtains the expression for the output kurtosis:

$$\kappa_z = 3\frac{\sum_p \left| \int H\left(f + \frac{p}{2T}\right) \cdot \left\{ \sum_k a_k a_{k-p}^* S_x\left(f + \frac{p-2k}{2T}\right) \right\} \cdot H^*\left(f - \frac{p}{2T}\right) df \right|^2}{\left| \int H(f) \cdot \left\{ \sum_k a_k a_k^* S_x\left(f - \frac{k}{T}\right) \right\} \cdot H^*(f)\, df \right|^2} \tag{6}$$

Note that for a narrowband system whose bandwidth is smaller than the frequency of the modulator, then $H\left(f + \frac{p}{2T}\right) H^*\left(f + \frac{p}{2T}\right)$ tends to zero and the output kurtosis tends towards 3.0. The proportion of bursts r_b and the waveform of the burst also plays an important role in the propagation of the nonstationary nature of the excitation in output of the linear system since they act on the Fourier coefficients a_k of the periodic modulation function.

4. Statistical rainflow counting and fatigue damage

The formulation for the distribution of peaks of a stationary Gaussian process of various bandwidths was initially found and published by S.O. Rice [11] and then largely relayed in the literature [5, 10]. The distribution of the peaks of a stationary Gaussian process is written:

$$f_G(s) = \frac{1}{\sigma}\left\{ \frac{\sqrt{1-\gamma^2}}{\sqrt{2\pi}} e^{\frac{-s^2}{2\sigma^2(1-\gamma^2)}} + \frac{s\gamma}{2\sigma} e^{\frac{-s^2}{2\sigma^2}} \left[1 + erf\left(\frac{s\gamma}{\sigma\sqrt{2(1-\gamma^2)}} \right) \right] \right\} \tag{7}$$

where σ is the root mean square (RMS) and γ is the irregularity factor as proposed by Rice [11]. It is defined as the ratio of the number of zero up-crossings in a time signal to the number of peaks. The irregularity factor tends to 1.0 for narrow-band signals and to 0.0 in a wideband case.

The peak distribution knowledge developed here is an extension of this theory for two classes of non-Gaussian processes: stationary and nonstationary leptokurtic processes.

4.1. Peak distribution in the case of a stationary leptokurtic process

The probability density function (PDF) of the random variable z can be obtained from the Gaussian PDF of the random variable x using the PDF transform [7,8]:

$$P_Z(z) = \frac{P_X(x)}{\left| dz/dx \right|} \tag{8}$$

Winterstein [15] proposed a monotonic function *g* acting as a zero-memory nonlinear system to model leptokurtic responses. It is based on Hermite polynomials to approach a non-Gaussian distribution and is well suited for mild deviations from a normal law. In the case of a zero mean, symmetric, standardized process *x*, the transformation *g* that allows one to obtain *z(t)* is:

$$z = g(x) = \sigma_x K \left[\frac{x}{\sigma_x} + \tilde{h}_4 \left(\left(\frac{x}{\sigma_x} \right)^3 - 3\frac{x}{\sigma_x} \right) \right] \tag{9}$$

with:

$$K = \frac{1}{\sqrt{1+6\tilde{h}_4^{\,2}}} \quad , \quad \tilde{h}_4 = \frac{\sqrt{1+1.5(\kappa-3)}-1}{18}$$

Where κ is the output kurtosis calculated in equation (4).
The inverse transform is [15]:

$$x = g^{-1}(z) = \sqrt[3]{\left(\frac{1}{2} \cdot \frac{z}{Kh_4\sigma_x} \right)^2 + \left(\frac{1-3h_4}{3h_4} \right)^3} - \sqrt[3]{\left(\frac{1}{2} \cdot \frac{z}{Kh_4\sigma_x} \right)^2 - \left(\frac{1-3h_4}{3h_4} \right)^3} \tag{10}$$

And the derivative of the transformation *g* is:

$$\frac{dz}{dx} = g'(x) = K(1-3\tilde{h}_4 + 3\frac{\tilde{h}_4}{\sigma_x^{\,2}} x^2) \tag{11}$$

The formulation can be successfully applied with the distribution of peaks $f_p(s)$. The distribution of peaks for the response *z* is hence obtained as:

$$f_p(s) = \frac{f_G(g^{-1}(s))}{\left| g'(g^{-1}(s)) \right|} \tag{12}$$

where f_p is the distribution of peaks for the response *z*, and f_G is the distribution of peaks for a Gaussian process having the RMS of the output signal, as defined in equation (7).

4.2. Peak distribution in the case of a nonstationary leptokurtic process

The output kurtosis for a cyclostationary excitation is given in Equation (6). The output signal is assumed to be of the same nature as the input signal i.e. amplitude modulated. The output signal is therefore made of a stationary Gaussian signal multiplied by a periodic, low frequency modulating signal. The output modulating function is assumed to have bursts made of the same waveform as in the input modulating function, occurring at the same rate but having a different amplitude due to the filtering process. Although, it is expected that the modulating function be distorted by the convolution, this assumption is practical and leads to good results compared to time domain simulations. The first objective is therefore to find the characteristics of the amplitude modulating signal i.e. the amplitude of the burst which is used to produce the calculated output kurtosis.

The peaks of the output signal are obtained by multiplying the peaks of the underlying stationary Gaussian signal by the modulating window. The distribution of the peaks of the output signal can therefore be calculated using the rule to find the PDF of the product of 2 independent random variables *X* and *A* [12] with distributions f_G and f_A respectively, given by Equation (13):

$$f_p(s) = \int_{-\infty}^{\infty} f_G(a) \frac{1}{|a|} f_A\left(\frac{s}{a}\right) da \tag{13}$$

with f_G the distribution of the peaks of the underlying stationary Gaussian signal (see equation (6)) and f_A the PDF of the modulating signal.This indeed requires an expression for the PDF of the modulating signal to be determined. This task is though straightforward for simple burst waveforms such as a sine wave, for example.

4.3. Distribution of rainflow ranges

The assumption is made that each peak is associated with a valley of similar magnitude and the cycle's range distribution can be determined from the peak distribution. Therefore, the cycle's range distribution - comparable to the rainflow cycle distribution - is deduced from the peak distribution, as per Equation (14).

$$f_R(S_R) = \frac{1}{2} f_p\left(\frac{S_R}{2}\right) \tag{14}$$

The use of equation (14) to calculate the range distribution is equivalent to considering that peaks and valleys are paired in the most severe way i.e. the highest peak goes with the lowest valley, the second highest peak goes with the second lowest valley, etc. This approach is therefore expected to be conservative in the case of a broadband response.

The distribution of stress ranges, comparable to a rainflow cycle histogram, can be calculated using equation (15):

$$N(S_R) = f_R(S_R).N_p.T \tag{15}$$

where T is the exposure duration and Np the total number of expected peaks (or ranges) per unit time. Np is calculated by using the second and fourth spectral moments of the response PSD [11].

The damage at a given stress range S_R is obtained as the ratio of the cycles counted at this stress range level to the number of cycles required to fail the component at this stress range level, which is given by the material curve like the one illustrated in Fig. 5. The total damage is obtained by summing the damage from each individual level of stress range using Miner's rule [19].

The SN curve may be made of several segments. Each segment is represented as a straight line in logarithmic space as described by the Basquin power-law relationship given in Equation (16).

$$C = N_f.S_R^{\ b} \tag{16}$$

where S_R is the stress range in MPa, N_f is the number of rainflow cycles to failure, C is the Basquin coefficient and

b is the Basquin exponent. Fatigue damage is determined by Equation (17).

$$D = \frac{1}{N_f} = \frac{1}{C}\int_0^{\infty} N\left(S_R\right).S_R{}^{b}.dS_R \tag{17}$$

D is the fatigue damage ratio. If $D \geq 1$ then the component is likely to fail within the test duration *T*. If $D<1$ then the fatigue life can be determined as T/D in seconds.

5. Application

5.1. The excitation signals

Table 1 shows an example PSD from the international standard MIL STD 810-G [3] corresponding to the general exposure to vibrations of to a jet aircraft cargo. The overall RMS vibration level is 4.02 g.

Table 1. PSD profile from MIL STD 810G [3]

Frequency (Hz)	Acceleration Spectral Density (g^2/Hz)
15	0.01
106	0.01
150	0.02
500	0.02
2000	0.0013
Global RMS = 4.02	

Fig. 6 shows example leptokurtic excitation signals with kurtosis = 10.0. Those signals were generated using the techniques introduced in this paper to produce stationary and nonstationary leptokurtic signals. They last 300 seconds and are sampled at 4096 points / sec. They have a frequency content corresponding to the PSD given in Table 1. they therefore share the same RMS value. Their PSDs are compared in Fig. 7.

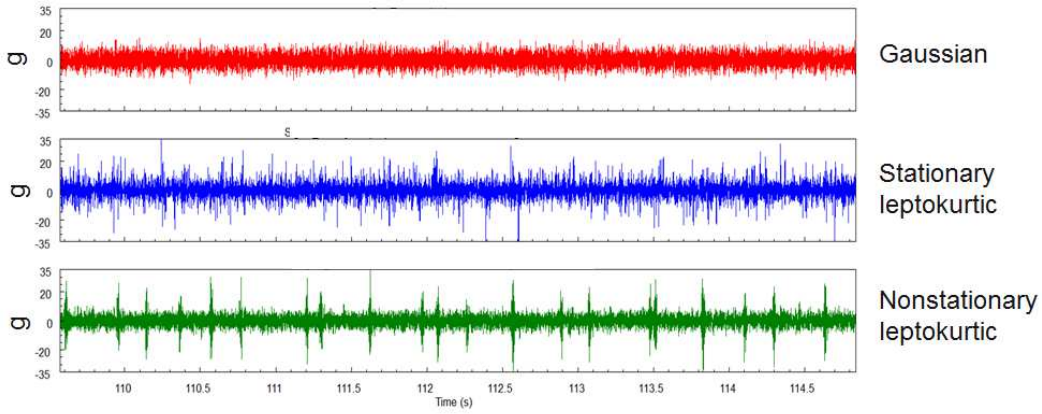

Fig. 6: Different excitation signals with similar PSD but either Gaussian or leptokurtic using the two described generation methods

Note the instantaneous peaks in the stationary leptokurtic case. In the nonstationary signal, the bursts are made of 0.03 seconds sinusoidal windows and there are 4 bursts per seconds; so the proportion of bursts is $r_b = 0.12$.

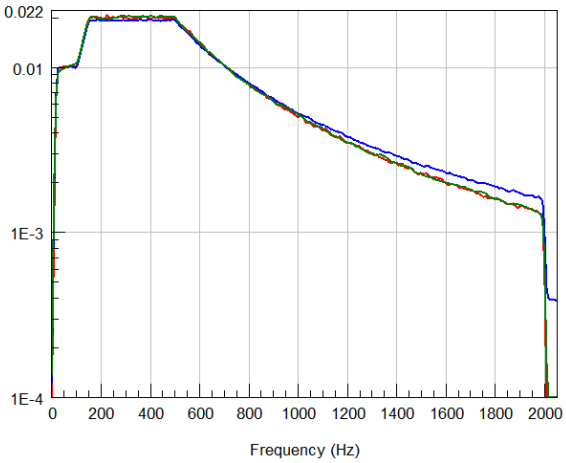

Fig. 7: PSD of Gaussian (red), stationary leptokurtic (blue) and nonstationary (green) signals

Note the harmonic distortion and the loss of dynamic range clearly seen in the high frequency region of the PSD of the stationary leptokurtic excitation. This is a known behavior of signals generated using zero-memory polynomial transformation [14].

5.2. The Linear Time-Invariant system

The LTI system chosen for this application is bimodal, with equal damping coefficients of 5%. The modulus of the frequency response function (FRF) is illustrated in Fig. 8.

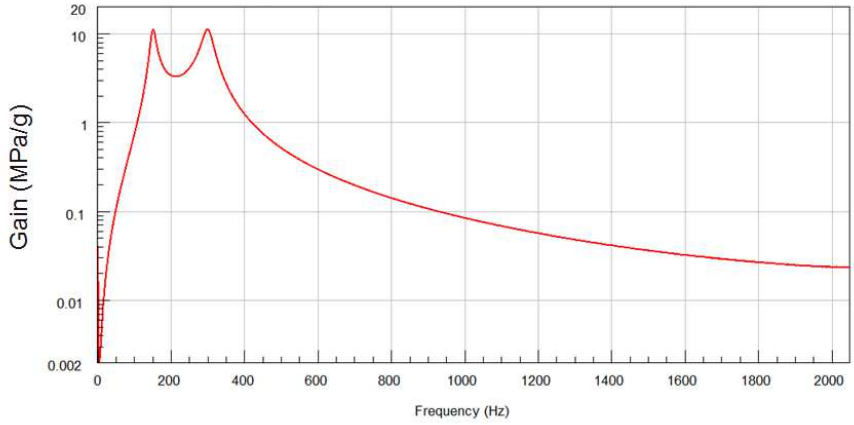

Fig. 8: Gain of the LTI's frequency response function

The obtained response PSDs computing from the various types of excitations are extremely similar and have the same RMS of ~13 MPa and irregularity coefficient of 0.58.

When the leptokurtic signals are used as excitation to the system, the output kurtosis is quite different, as

illustrated in Table 2:

Table 2. Comparison of the output statistics for various excitation signals.

	RMS		Kurtosis	
	Input RMS (g)	Output RMS (MPa)	Input Kurtosis	Output Kurtosis
Case of a Gaussian Excitation	4.02	13	3.0	3.0
Case of a stationary leptokurtic excitation	4.02	13	10.0	3.38
Case of a nonstationary leptokurtic excitation	4.02	13	10.0	7.43

The predicted output kurtosis – calculated using equations (4) and (6) - are 3.33 and 7.48 for the stationary and nonstationary case respectively, which is a very good match with the time domain simulations.

Clearly, the nonstationary case seems to allow more kurtosis to be propagated through the LTI system and seen in the output response signals. This result is not surprising: it is indeed expected that the instantaneous peaks in the stationary leptokurtic case be averaged out by the filtering process leading to a smaller kurtosis after filtering. In the nonstationary case, the well-separated bursts of higher energy are still present after filtering and the kurtosis remains at a similar level.

5.3. Peak distribution in the case of stationary leptokurtic excitations

Fig. 9 shows the peak distributions for the nonstationary signal (in blue). The distribution computed from the 300 seconds time domain realisation is in solid line, the theoretical distribution of peaks using equation (12) is in dotted line. For comparison purposes, the peak distribution for the equivalent Gaussian signal (of the same RMS) is shown in black dashed lines.

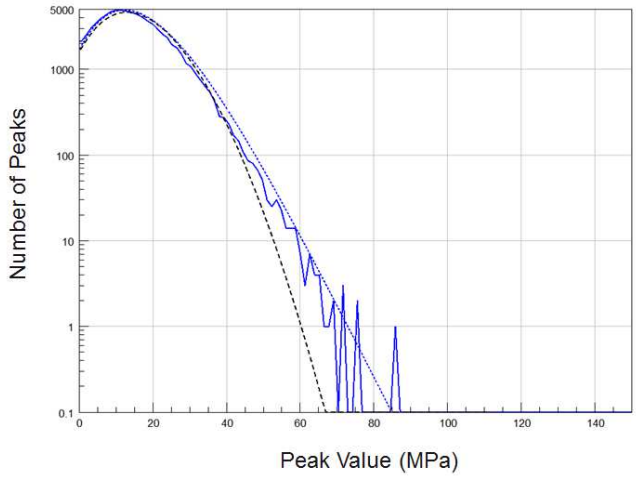

Fig. 9: Peak distributions for leptokurtic steady signals: theory (dotted blue) versus simulations (solid blue) and for the equivalent Gaussian signal

The theoretical peak distribution of the non-Gaussian response fits very well the distribution from the time domain realisation.

The peak distribution from the time domain simulations is quite close to the peak distribution of a Gaussian process, as expected from the low kurtosis value of 3.38. For instance, out of the 90 000 peaks counted, 750 have a value exceeding 3*RMS = 39 MPa in the Gaussian case, whereas 1000 peaks exceed 3*RMS in the case of the stationary leptokurtic response with kurtosis 3.38.

5.4. Peak distribution in the case of nonstationary leptokurtic excitations

Fig. 10 shows the peak distributions for the nonstationary signal (in red). The distribution computed from the 300 seconds time domain realisation is in solid line, the theoretical distribution of peaks using equation (13) is in dotted line. For comparison purposes, the peak distribution for the equivalent Gaussian signal (of the same RMS) is shown in black dashed lines.

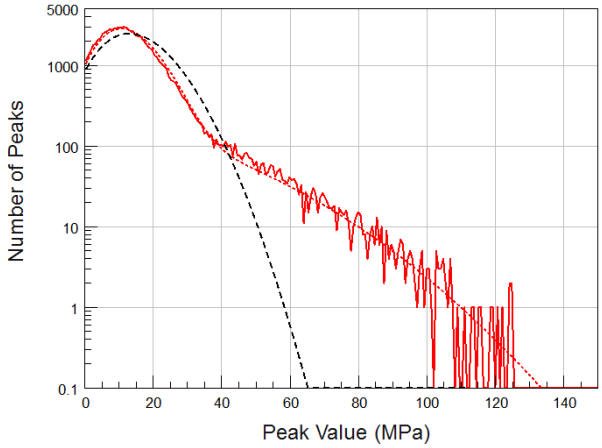

Fig. 10: Peak distributions for the nonstationary response signals: theory (dotted red) versus simulations (solid red) and for the equivalent Gaussian signal

The theoretical distribution of peaks fits very well the distribution from the time domain realisation. The peak distribution for the nonstationary signal shows a ticker tail, leading to a much higher probability of encountering high peaks than with the equivalent Gaussian signal (of same RMS). For instance, in the present case, out of the 90 000 peaks counted, almost 3000 have a value exceeding 3*RMS.

5.5. Comparison of the fatigue damage due to the various leptokurtic excitations

Fatigue damage is typically directly computed from the rainflow cycle histogram, which can be obtained from the time domain simulations or evaluated theoretically as per equation (15). Fig. 11 shows the rainflow cycle distributions for the Gaussian and the non-Gaussian stationary and nonstationary signals (in black, blue and red respectively). The distributions computed from the 300 seconds time domain realisations are in solid lines, the theoretical distributions of stress ranges are in dotted lines.

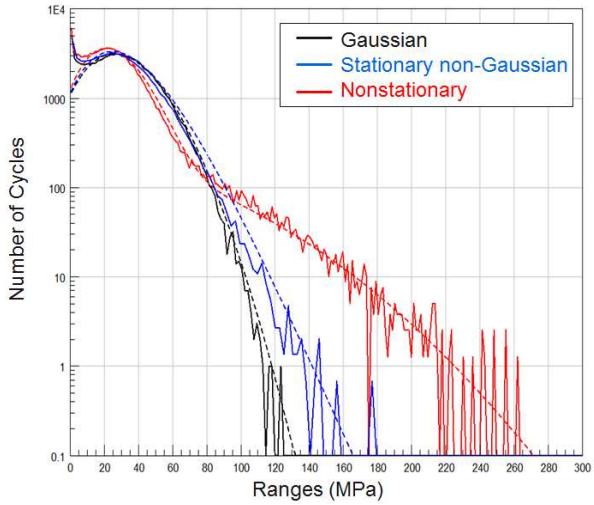

Fig. 11 rainflow cycle distributions for the Gaussian and the non-Gaussian stationary and nonstationary signals (in black, blue and red respectively)

The fatigue curve used (see Fig. 5 and Equation (16)) is for a typical value of the Basquin exponent of b=8 and stress range intercept C = 2000MPa. Table 3 shows the fatigue damage values calculated from the stress responses obtained when the system is exposed to the various excitations.

Table 3. Compare damage .

	Gaussian case	Case of a stationary leptokurtic excitation	Case of a nonstationary leptokurtic excitation
	Damage	Damage	Damage
From time domain simulations	2.2 x 10-8	1.1 x 10-7	2.4 x 10-6
From theoretical Rainflow distributions	2.7 x 10-8	1.6 x 10-7	2.6 x 10-6

The predicted damage values – calculated based on the theoretical rainflow cycle distributions - are quite comparable to the time domain simulations. The damage values from theoretical rainflow cycle distributions are slightly more conservative because of the perfect definition of the tail of the distribution, compared to the sparse content of the tails for the time domain data. This conservatism typically decreases with increased duration of the simulated time domain data.

Clearly, in the case of a nonstationary excitation, the resulting damage is dramatically higher than in the cases of a stationary Gaussian or even leptokurtic excitations.

6. Conclusions

Vibration endurance tests are used to qualify devices and validate that they can withstand the expected service loads. In many practical situations non-Gaussian tests are more realistic than Gaussian ones. With the help of modern controllers, the test engineer can set a kurtosis value to create excitation signals that are more impulsive in their nature and content.

There are several ways of generating a leptokurtic signal and two generic approaches were presented in this paper. The first produces a steady non-Gaussian excitation signal via the use of a zero-memory polynomial function. The latter generates a nonstationary excitation signal via amplitude modulation.

The paper shows that the kurtosis of the stress response obtained is very different depending on the type of leptokurtic excitation and the dynamics of the test article. Similarly, the stress peak distribution will also be quite different. Equations are obtained that give the ability to calculate reliably and accurately the response kurtosis and the stress peak distributions analytically, rather than needing long time domain response simulations.

It was shown that a nonstationary excitation generates higher stress level in the response compared to a stationary leptokurtic excitation of the same RMS and kurtosis value. As a consequence, nonstationary excitations produce more fatigue damage. The paper explains how to calculate the level of fatigue damage based on the stress peak distribution and the material fatigue curve.

An application case illustrates this by example. The calculated theoretical statistics and distributions are very comparable to the statistics and distributions obtained from time domain simulations.

The approach presented in this paper can be used in various applications. First, it allows a more accurate FEA-based fatigue simulation in the case where the vibration environment is known to be non-Gaussian. This leads to a more reliable design. Another interesting application is the reduction of the duration of endurance tests. Increasing the value of the kurtosis can be seen as an alternative approach to increasing the overall amplitudes for accelerated testing where an objective is to produce a reduction in the test duration.

References

[1] W. A.Gardner, The spectral correlation theory of cyclostationary time-series. Signal processing, 11(1), 13-36, 1986
[2] NATO Standardisation Agency, STANAG 4370. AECTP-200 (Edition 3). Mechanical Conditions, 2006
[3] USA Department of Defense, Test Method Standard Mil-Std-810G. Environmental Engineering Considerations and Laboratory Tests, 2008
[4] UK Ministry of Defence, Defence Standard 00-35 Issue 4. Environmental Handbook for Defence Materiel: Part 3: Environmental Test Methods, 2006
[5] J. S. Bendat, A. G.Piersol, Random Data: Analysis and Measurement Procedures, 3rd ed. John Wiley & Sons, New York, NY, 2000.
[6] F. Kihm, S. Rizzi, N. Ferguson, A. Halfpenny, Understanding how kurtosis is transferred from input acceleration to stress response and its influence on fatigue life. In, RASD 2013 , Pisa, IT, 01 - 03 Jul 2013. 16pp.
[7] K.A.Sweitzer, "Random vibration response statistics for fatigue analysis of nonlinear structures," Ph.D. Dissertation, Institute of Sound and Vibration Research, University of Southampton, UK, 2006.
[8] A. Papoulis, Probability, random variables, and stochastic processes (3rd edition), McGraw-Hill, Inc., 1991.
[9] Rizzi, S.A., Przekop, A., and Turner, T.L., "On the response of a nonlinear structure to high kurtosis non-Gaussian random loadings," EURODYN 2011, 8th International Conference on Structural Dynamics, Paper 41, Leuven, Belgium, July 4-6, 2011.
[10] Newland, D.E., An introduction to random vibrations and spectral analysis (2nd edition). New York, Longman Inc, 1984.
[11] Rice, S.O., "Mathematical analysis of random noise," Bell System Technical Journal, Vol. 23, pp. 282-332, 1944.
[12] Papoulis, A., "Narrow-band systems and Gaussianity," IEEE Transactions on Information Theory, Vol. 18, No. 1, pp. 20-27, 1972.
[13] W.A. Gardner, A. Napolitano, L. Paura, Cyclostationarity: Half a century of research, Signal Processing 86(4):639-697 · April 2006
[14] Steinwolf, A., "Two methods for random shaker testing with low kurtosis," Sound & Vibration, pp. 18-22, October, 2008.
[15] S.R., Winterstein., "Nonlinear vibration models for extremes and fatigue," ASCE Journal of Engineering Mechanics, Vol. 114, No. 10, pp. 1772-1790, 1988.
[16] Smallwood, D.O., "Vibration with non-Gaussian noise," Journal of the Institute of Environmental Sciences and Technology, Vol. 52, No. 3, pp. 13-30, 2009.
[17] J Antoni , INSA , Lyon. Personal communication. Laboratoire Vibrations Acoustique, University of Lyon, France.
[18] A. Halfpenny, "Rainflow cycle counting and fatigue analysis from PSD," Proceedings of the ASTELAB Conference, Paris, France, September 25 – 27, 2007.
[19] M.A.Miner, "Cumulative damage in fatigue," Trans. ASME, Journal of Applied Mechanics, Vol. 67, pp. A159-A164, 1945.
[20] J. Antoni, Cyclostationarity by examples, Mechanical Systems and Signal Processing, Volume 23, Issue 4, May 2009, Pages 987-1036, ISSN 0888-3270